The structure and electron energy loss near edge structure of tungsten oxide thin films prepared by pulsed cathodic arc deposition and plasma-assisted pulsed magnetron sputtering

M R Field[1], D G McCulloch[1], S N H Lim[2], A Anders[3], V J Keast[4] and R W Burgess[4]

[1]Applied Physics, School of Applied Sciences, RMIT University, GPO Box 2476V, Melbourne 3001, Australia

[2] School of Physics, University of Sydney, NSW 2006, Australia

[3] Lawrence Berkeley National Laboratory, University of California, 1 Cyclotron Road, Berkeley, California 94720

[4] School of Mathematical and Physical Sciences, The University of Newcastle, Callaghan NSW 2308, Australia

Abstract.

The microstructure and energy-loss near-edge structure (ELNES) of pulsed cathodic arc and pulsed magnetron sputtered WO_3 thin films were investigated. It was found that the cathodic arc deposited material consisted of the α-WO_3 phase with a high degree of crystallinity. In contrast, the magnetron sputtered material was highly disordered making it difficult to determine its phase. A self-consistent real space multiple scattering approach was used to calculate the NES of the various phases of WO_3. Each phase was found to exhibit a unique NES allowing different phases of WO_3 to be identified. The real space approach also allowed the origin of the main features in the NES to be investigated as the cluster size increased. The calculated NES for the room temperature γ-WO_3 was found to compare well to previous X-ray absorption spectra and to NES obtained by full-potential band structure calculation.

1. Introduction

Tungsten tri-oxide (WO_3) is an important transparent conducting oxide which exhibits interesting chromogenic properties allowing the material to reversibly change its optical state. This property is being investigated for "smart windows", electro-optical components and display applications [1-3]. It can be deposited using several methods including sputtering [1, 2], evaporation [4, 5], pulsed laser deposition [6] and cathodic arc deposition [7]. In general, the microstructure and performance of the films depends on the method, deposition temperature and other process conditions, with both amorphous and polycrystalline materials reported [8]. Crystalline WO_3 is known to have a perovskite-type structure which undergoes up to 4 phase changes depending on the temperature [9]. Starting with a monoclinic (ε) phase at low temperatures [10], the structure transforms into either a triclinic (δ) [9, 11] or a different monoclinic phase (γ) [9, 11] at room temperature. At higher temperatures, orthorhombic (β) [12] and tetragonal (α) [13] phases occur at 480°C and 770°C, respectively. Although all phases are based on distorted WO_6 octahedra, each structure is subtly different and these differences could influence the electronic and other properties

In this paper we investigate the microstructure of WO_3 thin films prepared using two different techniques: pulsed magnetron sputtering and pulsed cathodic arc deposition. The differences between these two techniques are significant. Cathodic arc deposited films are formed from energetic and multiply charged ions [14-16] while sputtered films are deposited primarily from low energy neutrals [17], though energetic negative ions may be present [18]. The incident energy of the depositing particles is known to have an important influence on the microstructure [19, 20].

We employ transmission electron microscopy (TEM) and electron energy-loss spectroscopy (EELS) to characterize the films. Superimposed on each EELS absorption edge is structure (known as energy loss near-edge structure or ELNES) which arises because the final state wave function of the excited electron is modified by chemical bonding. This fine structure is identical to, and has its origin in the same process as the X-ray absorption near-edge structure (XANES). Therefore, the

ELNES/XANES may provide a convenient way of distinguishing between the various phases of WO_3. However, the interpretation of ELNES is not straight forward and accurate theoretical modelling is essential [21]. We therefore employ the FEFF8.2 code, a real space multiple scattering code, to calculate the ELNES of several possible WO_3 structures to compare with experiment. To validate our calculations, we compare the results to previous X-ray absorption spectra and band structure calculations performed using WIEN2k [22].

2. Experimental

Films of WO_3 were prepared by pulsed magnetron sputtering and pulsed cathodic arc deposition.

For the magnetron deposition experiments, the chamber was initially pumped down to a base pressure of about 1.3 x 10^{-6} Torr (1.7 x 10^{-4} Pa) using a cryogenic pump with a pumping speed of 1500 l/s. The pumping speed was reduced using an adjustable gate valve to obtain a relatively high total pressure of 42 mTorr (5.6 Pa) with Ar and O_2 gas flows of 50 and 40 sccm, respectively. The gas was introduced into a gas plasma source of the constricted plasma source type [23] operated with a Pinnacle Plus power supply at 1500 W (pulsed-DC, 100 kHz, 1 μs reverse time). It was noted that the total pressure was reduced to about 36 mTorr (4.8 Pa) during deposition, which is due to the consumption of oxygen by the growing film. A 3" (76 mm) diameter W target with a sputter power of 1200 W was used. The substrate was placed 90 mm away from the sputtering gun and the plasma source. Total deposition time was 10 mins.

For the pulsed cathodic arc deposition experiment, the chamber was pumped down to a base pressure of about 7 x 10^{-6} Torr (9 x 10^{-4} Pa) and backfilled with O_2 at a flow rate of 10 sccm to a pressure of about 6.6 mTorr (0.88 Pa). The pulsed arc source [24], equipped with a tungsten rod cathode and a 90° open-coil macroparticle filter, was fed from a switched capacitor bank (0.3 F) charged to 270 V, resulting in an arc current of about 180 A, limited by a 1.5 Ω resistor in series. The arc repetition rate was 3 pulses per second, with an arc duration of 3 ms. After 7600 pulses, a film thickness of 200 nm was obtained, with the holder placed about 90 mm from the filter exit.

Throughout the deposition process, the sample holder was pulsed-biased to -200 V with a pulse cycle of 10 μs on (-200 V) and 90 μs off (ground).

The stoichiometry of the films were measured using X-ray Photoelectron Spectroscopy (XPS) performed on a VG Microlab 310F with a dual Al/Mg anode unmonochromated X-ray source operated at a power of 300 W and 15 kV excitation voltage. The sample was tilted such that the electron analyzer normal to the sample surface collected the escaping electrons. The analyzed area is determined by the electrostatic lens and slits of the analyzer and in this case was approximately a rectangular area of 5 x 1 mm^2. Cross-section TEM specimens of the samples were prepared using mechanical polishing and ion beam thinning. These specimens were then analysed in a JEOL2010 TEM operating at 200 kV. To measure the Energy Loss NES (ELNES), EELS spectra of the coatings were collected using a Gatan Imaging Filter operating in spectroscopy mode. The energy resolution was 1.8 eV as measured by the FWHM of the zero loss peak. All spectra were collected in imaging mode with a spectrometer entrance aperture of 2 mm.

3. Theoretical

The ELNES on the O K-edge for several possible WO_3 phases was calculated using the FEFF8.2 code [25] (which will be referred to as FEFF8 throughout this paper). FEFF8 is a real-space multiple scattering code which employs accurate self-consistent-field potentials to calculate the edge structure. Other features in the code include an energy dependent exchange correlation potential, the ability to use screened core holes and Debye-Waller factors to treat the effects of vibrations. A multiple scattering Path Expansion is used to calculate the ELNES for a cluster of atoms. Several WO_3 phases were simulated using the parameters in table I. For all calculations, the exchange potential used was the Hedin–Lundqvist type which is recommended for solids. Each of the WO_3 structures listed in table I has at least 2 unique oxygen positions. Therefore, the NES of each unique oxygen atom was modelled separately and then combined to provide an average.

Calculations of the O K-edges were also performed using the WIEN2k code [26] on the tetragonal α-WO_3 phase and the monoclinic γ-WO_3 phase. The electron wavefunctions and eigenvalues are calculated by the full-potential (linearized) augmented plane-wave ((L)APW) + local orbitals (lo) method. Exchange and correlation effects were treated using the generalized gradient approximation (GGA). The plane wave cut-off ($R_{MT}K_{MAX}$) was set to 7. The muffin tin radii were chosen as large as possible but without overlapping spheres. The number of k-points in the irreducible Brillouin zone (BZ) was 90 for α-WO_3 and 54 for γ-WO_3 . Convergence tests showed that this number of k-points were adequate. A core-hole was not included as i's effect was found to be a relatively small change in the intensity of the peaks, but with a considerable increase in computational time. The ELNES (XANES) was calculated using the XSPEC subroutine within WIEN2k. Spectra were calculated for all inequivalent positions in the unit cell and an appropriate average taken. Differences between the different atomic sites were very small. Lorentzian broadening of 1.3 eV was included to account for the experimental energy resolution.

Table 1: Details of the phases and cluster parameters used in the FEFF8 calculations.

Structure	Symmetry	Space Group	Lattice Parameters	Cluster Size	FMS Radius
α–WO_3 [13]	Tetragonal	P4/nmm	a_o=5.3031Å c_o=3.9348	161 atoms	6Å
β-WO_3 [12]	Orthorhombic	Pmnb	a_o=7.341Å b_o=7.570Å c_o=7.754 Å	179 atoms	6Å
γ-WO_3 [11]	Monoclinic	$P2_1/n$	a_o=7.30084 b_o=7.53889 c_o=7.68962 $\alpha=\gamma$=90° β= 90.892°	165 atoms	6Å
δ-WO_3 [11]	Triclinic	$P\bar{1}$	a_o=7.31278Å b_o=7.52540Å c_o=7.68954Å α=88.847° β=90.912° γ=90.940°	172 atoms	6Å
ε-WO_3 [10]	Monoclinic	Pc	a_o=5.27710Å b_o=5.15541Å c_o=7.66297Å β=91.97592°	167 atoms	6.96Å

3. Results and Discussion

The stoichiometry of the sputtered and cathodic arc deposited films was determined using XPS was $WO_{2.87}$ and $WO_{2.73}$, respectively. Therefore, both films are close to stoichiometric. The corresponding cross-sectional TEM images of these samples are shown in Fig. 1 (a) and (b). These images show the glass substrate on the left and the film running down the middle of the image. The microstructure of the sputtered film appeared highly disordered and this was confirmed by the selected area diffraction pattern shown in Fig. 2(a). It was not possible to index this diffraction pattern unambiguously to any particular phase. The arc deposited film was highly ordered, and the insert in Figure 1(b) is a high resolution image which reveals a crystal lattice. The selected area diffraction pattern from a region of this film is shown in figure 2(b). The pattern has been indexed to the α-WO_3 phase. This is an interesting result given that previous investigations of tungsten oxide films prepared using physical deposition methods have exhibited a γ–WO_3 structure [8]. The energetic plasma associated with cathodic arc deposition clearly had an impact on the microstructure on the resulting WO_3 producing the high temperature α-phase and improved crystallinity.

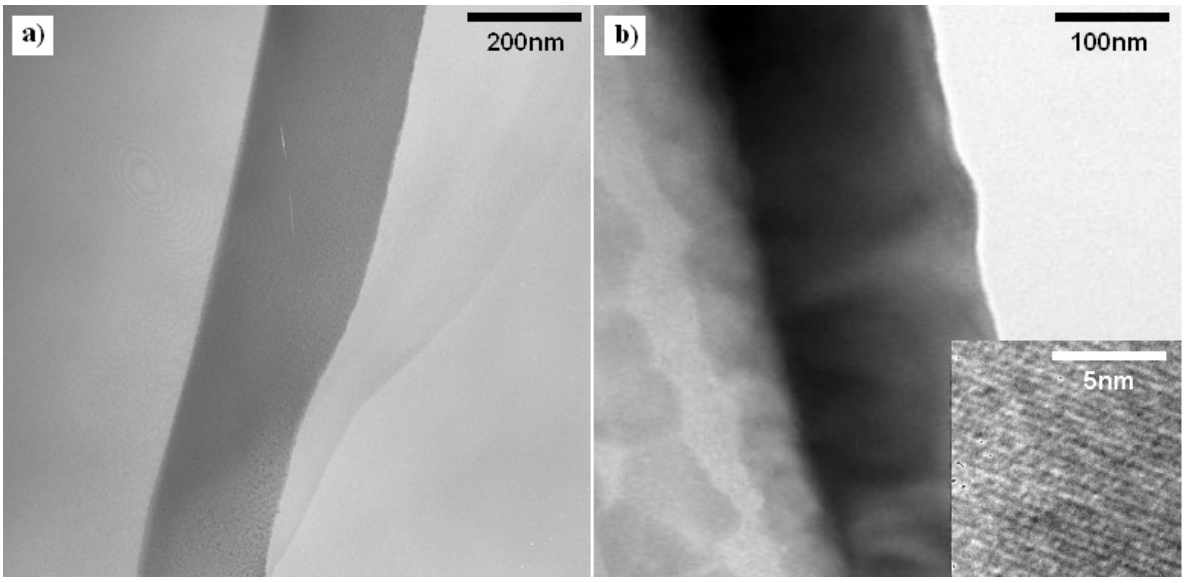

Figure 1: Cross sectional TEM Images of the deposited films. a) Magnetron sputtered sample b) Cathodic arc sample. Insert: high resolution image of sputtered sample.

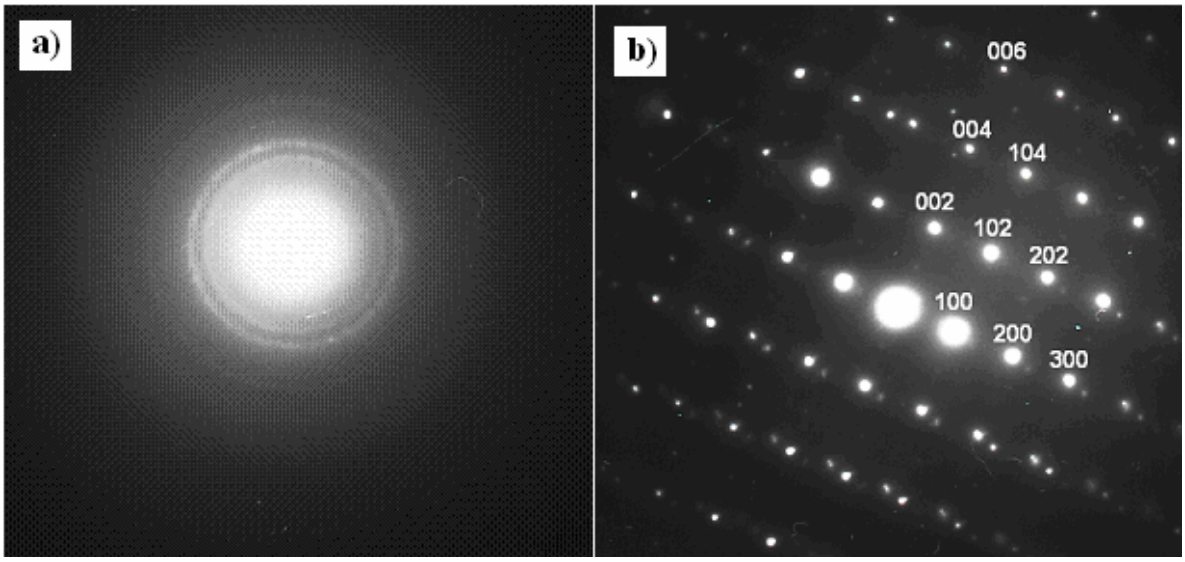

Figure 2: Selected area diffraction patterns of the (a) magnetron sputtered and (b) cathodic arc films shown in Figure 1. The diffraction pattern in (b) has been indexed to the α-WO_3.

In figure 3 we compare the oxygen K-edges obtained using EELS from the magnetron sputtered and the cathodic arc deposited coatings. The features in the ELNES of the magnetron sputtered sample are broad, probably the result of the high level of disorder in this sample. In contrast, the fine structure in the cathodic arc sample is more distinct and shows an additional peak at 556.7eV (labelled "G" in the figure).

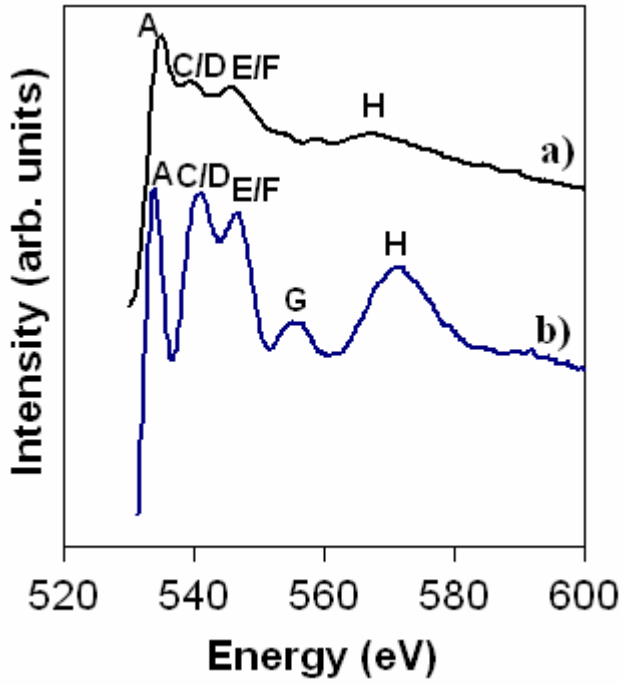

Figure 3: Oxygen K-edge EELS spectra for the 2 experimental samples. (a) Magnetron Sputtered ELNES (b) Cathodic Arc ELNES.

Figure 4a) compares the O K-edge of γ-WO_3 calculated using FEFF8 and that obtained using WIEN2k plotted from the Fermi energy. Also shown is the O K-edge obtained using XANES for a sputtered WO_3 film which was identified as being γ-WO_3 [8]. Overall, the results are similar with the main features reproduced using both methods. The FEFF8 calculation does include the first extended fine structure peak at approximately 45eV. Also notable is that the doublet at approximately 15 eV is not resolved in WIEN2k calculation.

In a similar way, Figure 4b) compares the O K-edge of α-WO_3 collected using EELS in this work to calculations made with FEFF8 and WIEN2k.

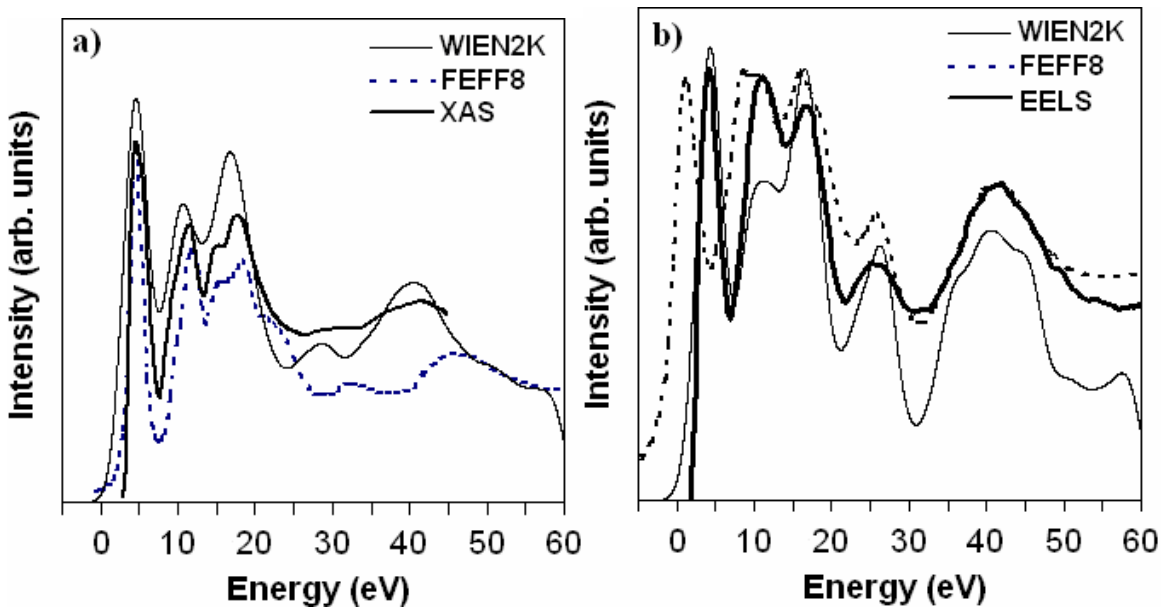

Figure 4: Comparison of the O K-edge of calculated using FEFF8 and WIEN2k. Note that the energy scale is relative to the Fermi energy. These are compared to a) γ-WO_3 obtained using X-ray absorption spectroscopy [8] and b) α-WO_3 obtained using EELS.

Figure 5 shows a comparison of the NES of the oxygen k-edges for each phase of WO_3 calculated using FEFF8 with 0.5eV of broadening added to the calculation. In order to match the experiment, the first extended fine structure peak (H) was aligned to 573.3eV, as was measured in the case of the arc deposited sample. Clearly, each phase has a unique NES reflecting their different microstructures. Similarities between the NES can be seen, most notable between the γ-WO_3 and ε-WO_3 phases, which are both monoclinic.

Table 2 lists the energies of the main features (labelled in figure 5) found in the FEFF8 calculations. Generally, the energies of the features do not vary significantly between the phases, although the relative intensities do. Table 2 also shows the positions of features which could be resolved from the experimental work shown in figure 3. Due to experimental broadening, particularly in the EELS measurements, some adjacent features are not resolved and appear as a single peak. Where appropriate, features have been labelled in figure 3.

The broadness of the features in our magnetron sputtered sample makes it difficult to assign a phase. As diffraction data indicated that the cathodic arc deposited sample was the tetragonal phase, the NES for the α-WO_3 case with 1.3eV broadening was overlayed with the collected EELS spectra (shown as a dotted line in figure 3(b)). There is a good correlation between the calculated peak positions and the collected EELS spectra, although there is an error (of approximately 3 eV) in the position of peak A. This peak reflects the oxygen 2p-states in the conduction band formed by 5d tungsten and 2p oxygen hybrid orbitals [8]. Previous work has shown that the position of the peak near the edge offset in transition metal oxides can shift due to the influence of quadrupole effects [27] which were not included in these calculations. However, the inclusion of quadrupole transitions for the case of α-WO_3 only resulted in a lowering the relative intensity of this feature. The discrepancy in the position of peak A may be the result of errors in the calculation of the potential, the accuracy of which is critical for reproducing features with energies within approximately 10eV of the threshold [27]. This is confirmed by the full-potential calculations of WIEN2k, which predict the correct energy for this peak.

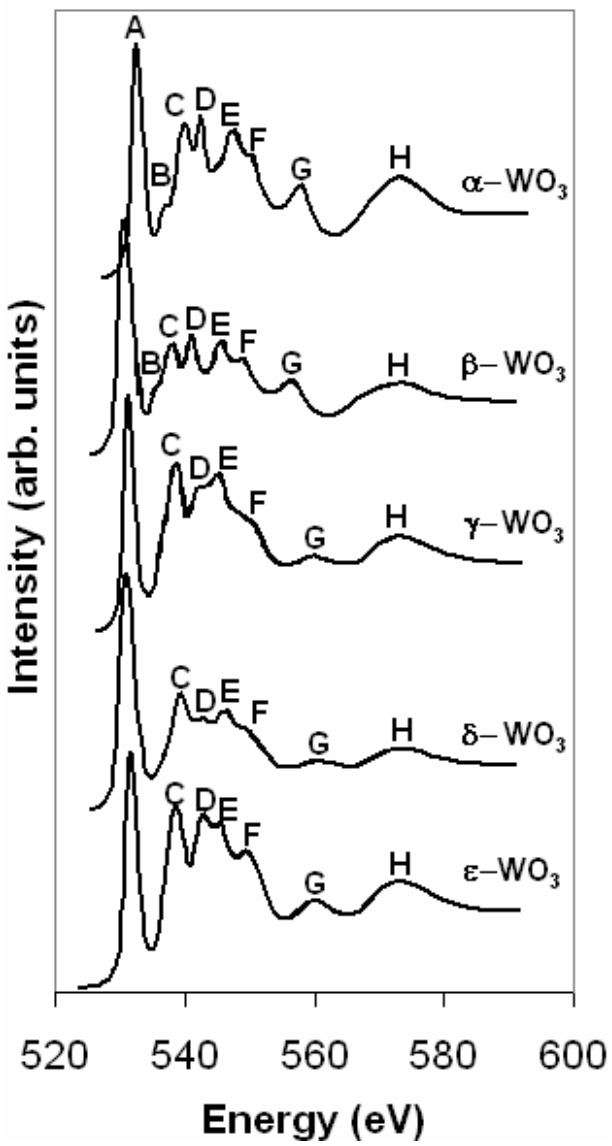

Figure 5: The calculated oxygen K-edge NES for the known phases of WO_3. The main features have been labelled and their energies have been listed in Table 2.

Table 2: Energy (eV) of the main features in both the experimental and FEFF8 calculated O K-edges. Note that the calculated values have been shifted so that the first extended fine structure peak (H) aligns with that of the cathodic arc deposited material.

Sample /Phase	A	B	C	D	E	F	G	H*	Shift (eV)
Magnetron Sputtered	535.4	-	540.2		546.5		-	568.1	-
Cathodic Arc	535.7	-	542.5		548.1		556.7	573.3	-
α	532.7	537.0	539.9	542.3	547.3	550.2	557.8	573.3	8.6
β	530.8	536.0	538.2	541.0	545.7	548.8	556.3	573.3	6.7
γ	531.7	536.8	538.6	542.0	545.3	550.9	559.7	573.3	7.6
δ	531.2	-	539.1	542.5	546.2	548.9	560.1	573.3	8.1
ε	531.8	-	538.6	542.8	545.4	549.7	559.9	573.3	7.7

The real space approach employed in FEFF8 allows us to explore the variation in NES as a function of cluster size around the absorbing atom. Figure 6 shows the variation in NES as the cluster size increases. Also shown in the figure are structural models for various clusters which give rise to significant changes in the NES. The basic edge shape is formed for a small cluster consisting of an oxygen atom bonded to its 2 adjacent tungsten atoms. The dominant first peak (A) appears when the absorbing oxygen atom is surrounded by its 8 nearest oxygen atoms, 4 from each adjoining octahedral unit. The next significant change in the NES occurs for a cluster size of 12 atoms, when the two adjoining octahedral units are completed and peaks C/D and E/F form.

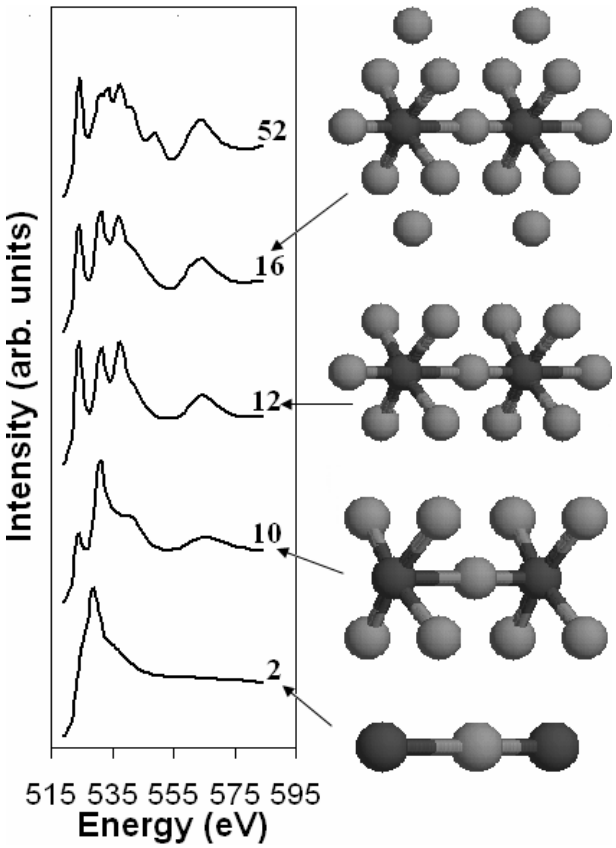

Figure 6: Calculated NES of the oxygen K-edge for the α-WO_3 phase for various numbers of atoms surrounding the absorbing oxygen (left). A graphical representation of the clusters is also shown (right).

Conclusion

The structure of tungsten trioxide thin films was found to depend on the fabrication method. The energetic beam associated with cathodic arc deposition produced a film with a well-ordered tetragonal structure. On the other hand, magnetron sputtering produced a highly disordered material which due to the limited energy resolution of EELS was difficult to assign to a particular phase. It was shown that the FEFF8 code is able to distinguish subtle differences in the oxygen k-edge NES for various phases of WO_3. The calculated NES using both FEFF8 and WIEN2k for the γ-WO_3 phase was found to match well with previous published experiment X-ray absorption results. There was also a good match between the calculated α-WO_3 NES and that found using EELS for the cathodic deposited film.

References

1. **Cui, H.N., et al., *Electrochromic coatings for smart windows.* Surface Science Proceedings of the 7th International Conference on Nanometer-Scale Science and Technology and the 21st European Conference on Surface Science, 2003. 532-535: p. 1127-1131.**
2. **Akl, A.A., H. Kamal, and K. Abdel-Hady, *Characterization of tungsten oxide films of different crystallinity prepared by RF sputtering.* Physica B: Condensed Matter, 2003. 325: p. 65-75.**
3. **Granqvist, C.G., *Handbook of Inorganic Electrochromic Materials*. 1995, Amsterdam: Elsevier.**
4. **Gillet, M., A. Al-Mohammad, and C. Lemire, *Microstructural analysis of WO3 thin films on alumina substrates.* Thin Solid Films, 2002. 410(1-2): p. 194-199.**
5. **Shigesato, Y., et al., *Characterization of evaporated amorphous WO3 films by Raman and FTIR spectroscopies.* Applied Surface Science, 1988. 33-34: p. 804-811.**
6. **Rougier, A., et al., *Characterization of pulsed laser deposited WO3 thin films for electrochromic devices.* Applied Surface Science, 1999. 153(1): p. 1-9.**
7. **Tay, B.K., Z.W. Zhao, and D.H.C. Chua, *Review of metal oxide films deposited by filtered cathodic vacuum arc technique.* Materials Science and Engineering: R: Reports, 2006. 52(1-3): p. 1-48.**
8. **Purans, J., et al., *X-ray absorption study of the electronic structure of tungsten and molybdenum oxides on the O K-edge.* Electrochimica Acta, 2001. 46(13-14): p. 1973-1976.**
9. **Aird, A., et al., *Sheet superconductivity in : crystal structure of the tetragonal matrix.* Journal of Physics: Condensed Matter, 1998. 10(33): p. L569-L574.**
10. **Salje, E.K.H., et al., *Crystal structure and paramagnetic behaviour of ε-WO_{3-x}.* Journal of Physics: Condensed Matter, 1997. 9(31): p. 6563-6577.**
11. **Woodward, P.M., A.W. Sleight, and T. Vogt, *Structure refinement of triclinic tungsten trioxide.* Journal of Physics and Chemistry of Solids, 1995. 56(10): p. 1305-1315.**
12. **Salje, E., *The orthorhombic phase of WO3.* Acta Crystallographica Section B, 1977. 33: p. 574-577.**
13. **Locherer, K.R., I.P. Swainson, and E.K.H. Salje, *Transition to a new tetragonal phase of WO3: crystal structure and distortion parameters.* Journal of Physics: Condensed Matter, 1999. 11(21): p. 4143-4156.**
14. **Anders, A., *Ion charge state distributions of vacuum arc plasmas: The origin of species.* Physical Review E, 1997. 55(1): p. 969-981.**
15. **Oks, E.M., A. Anders, and I.G. Brown, *Ion charge state distributions in high current vacuum arc plasmas in a magnetic field.* IEEE Transactions on Plasma Science, 1996. 24(3): p. 1174-1183.**
16. **Anders, A. and G.Y. Yushkov, *Ion flux from vacuum arc cathode spots in the absence and presence of a magnetic field.* Journal of Applied Physics, 2002. 91(8): p. 4824-4832.**
17. **Mattox, D.M., *Handbook of physical vapor deposition (PVD) processing*. 1998: Noyes Publications.**
18. **Mráz, S. and J.M. Schneider, *Energy distribution of O- ions during reactive magnetron sputtering.* Applied Physics Letters, 2006. 89(5): p. 051502**
19. **Bilek, M.M.M., et al., *Control of stress and microstructure in cathodic arc deposited films.* IEEE Transactions on Plasma Science, 2002. 31(5): p. 939-944.**

20. **Brown, I.G., *Cathodic Arc Deposition of Films.* Annual Review Material Science., 1998. 28: p. 243-269.**
21. **Keast, V.J., et al., *Electron energy-loss near-edge structure â€“ a tool for the investigation of electronic structure on the nanometre scale.* Journal of Microscopy, 2001. 203(2): p. 135-175.**
22. **Schwarz, K., P. Blaha, and G.K.H. Madsen, *Electronic structure calculations of solids using the WIEN2k package for material sciences.* Computer Physics Communications, 2002. 147(1-2): p. 71-76.**
23. **Anders, A. and G.Y. Yushkov, *Low-energy linear oxygen plasma source.* Review of Scientific Instruments, 2007. 78(4): p. 043304-7.**
24. **MacGill, R.A., et al. *Streaming metal plasma generation by vacuum arc plasma guns*. in *Proceedings of the 7th international conference on ion sources*. 1998. Shirahama, Wakayama (Japan): AIP.**
25. **Ravel, B., *FEFF*. http://leonardo.phys.washington.edu/feff/.**
26. **Hebert, C., *Practical aspects of running the WIEN2k code for electron spectroscopy.* Micron, 2007. 38(1): p. 12-28.**
27. **Modrow, H., et al., *Calculation and interpretation of K-shell x-ray absorption near-edge structure of transition metal oxides.* Physical Review B, 2003. 67(3): p. 035123.**